ELSEVIER

Polymer 42 (2001) 1525–1532

polymer

www.elsevier.nl/locate/polymer

Polycyanurates modified with hydroxyl-terminated or cyanated poly(ether sulfone)

Jer-Yuan Chang[a], Jin-Long Hong[b,*]

[a]*Department of Chemical Engineering, Yung-Ta Junior College of Technology and Commerce, Ping-Tung, Taiwan 90424, ROC*
[b]*Institute of Materials Science and Engineering, National Sun Yat-Sen University, Kaohsiung, Taiwan 80424, ROC*

Received 18 January 2000; received in revised form 29 May 2000; accepted 5 June 2000

Abstract

Polycyanurates generated from polycyclotrimerization of bisphenol A dicyanate (BPADCy) were blended with either hydroxyl-terminated or cyanated poly(ether sulfone) (as HPES or CPES, respectively) to improve their mechanical properties. Results from scanning electron microscopy suggest a discrete-continuous fracture surface for the polycyanurate blended with 10 wt% of HPES; but for the CPES-blended polycyanurate, a blurring interface between particle and matrix was observed. The blurring interface was originated from inter-reactions through the cyanate groups in CPES and BPADCy. This blurring interface can also be generated if 1 wt% of catalyst system (*n*-nonylphenol/cobaltic acetylacetonate) was used during cure of mixtures of HPES and BPADCy. This blurring interface in the catalyzed system is attributed to the chemical reaction between the hydroxyl termini in HPES and the cyanate groups in BPADCy. The discrete particle sizes in the cured HPES/BPADCy strongly depend on the curing temperatures. With a higher curing temperature, a larger average particle size was generated.

Keywords: Polycyanurate; Poly(ether sulfone); Blend

1. Introduction

Thermosetting polycyanurates prepared from polycyclotrimerization [1,2] of aromatic dicyanates have drawn increasing attention due to their important application in industry. As shown in Fig. 1, the resulting polycyanurates have crosslinked structure with *s*-triazine rings as interconnected junction points. This crosslinked polycyanurates distinguishes themselves from other crosslinked polymers by the excellent dielectric properties, thermal and dimensional stability [3–5] that facilitated their applications in the area of circuit board fabrications [6]. Nevertheless, polycyanurates with their high crosslinking density are generally poor in the impact resistance.

To improve the mechanical properties, thermoplastics such as polycarbonate, poly(ethtylene terephthalate), polysulfone and poly(ether imide), had been used to toughen the polycyanurates [7–13]. Among them, Pascault et al. [11] studied the effect of poly(ether sulfone) on the curing rates of two commercial aromatic dicyanates. Woo et al. [12,13] described the relationship between the thermoplastics content and the resulting morphology in a poly(aryl sulfone)/bisphenol-E dicyanate system. The blends exhibited a simple matrix–domain morphology with the polycyanurate as the continuous phase if the volume content of the poly(aryl sulfone) is less than 10%; however, phase inversion occurred and the thermoplastic poly(aryl sulfone) becomes the continuous phase when its content is more than 20%. This research gave detailed study on morphology and stimulated our interest for this topic.

For a thermoplastic-modified crosslinked system, manipulations of the curing rate and the phase separation process are critical for the final morphology. It means that phase separation developed before any process leading to structure lock-in (e.g. gel formation or vitrification) would eventually determine the final morphology. In addition, various reaction parameters (e.g. curing temperature) should be well understood in order to tailor the final properties. In this research, different mixtures of poly(ether sulfone)/bisphenol A dicyanate (BPADCy) were cured and their resulting morphology in relationship to the constitutive components were investigated. Three experimental variables were concerned in this study. Firstly, hydroxyl-terminated and cyanated poly(ether sulfone)s (as HPES and CPES shown in Fig. 1) were used to co-cure with BPADCy to evaluate the effect of terminal groups on the final morphologies of the cured products. Secondly, temperature is an important

* Corresponding author. Tel.: +886-7-525-2000; fax: +886-7-525-4099.
E-mail address: jlhong@mail.nsysu.edu.tw (J.-L. Hong).

0032-3861/01/$ - see front matter
PII: S0032-3861(00)00415-8

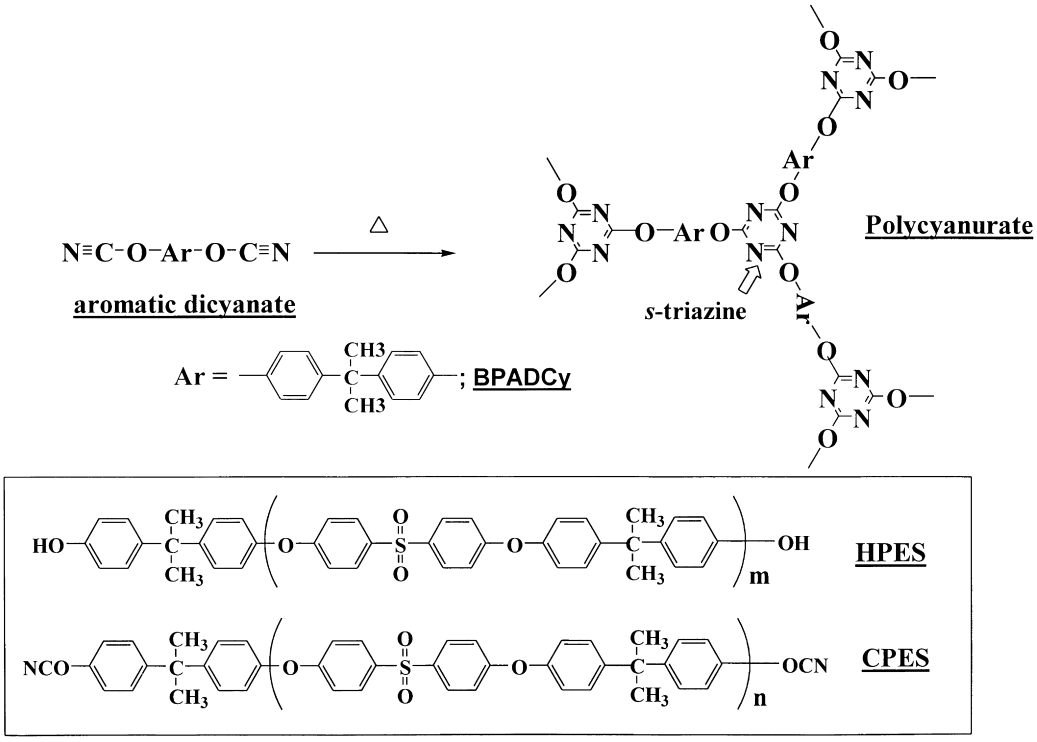

Fig. 1. Polycyclotrimerizations of aromatic dicyanates to form polycyanurates with *s*-triazine crosslinked points and the chemical structures of hydroxyl-terminated and cyanated poly(ether sulfone)s (as HPES and CPES).

factor on controlling the curing rate and the final morphology of the cured product; therefore, cure of BPADCy/HPES blend at different temperatures was also carried out in this research. Thirdly, a catalyst system, cobalt acetylacetonate)/*n*-nonyl phenol (CA/NP), was used to accelerate the curing reaction and the morphology of the cured product was found to be interesting. In this study, scanning and transmission electron microscopies (SEM and TEM) were applied to investigate the morphological variations. In addition, differential scanning calorimetry (DSC) and Fourier transformation infrared spectroscopy (FTIR) were used in this study for the characterizations of thermal properties and chemical structures of the cured products, respectively.

2. Experimental

2.1. Materials and synthesis

Bisphenol A dicyanate (Tokyo Chemical Inc.) was used without further purification. The solvent used for preparation of miscible blends, methylene chloride, was distilled under nitrogen atmosphere and stored over molecular sieve. The syntheses of HPESs and CPESs were described previously [14]. The number-average molecular weights of HPESs and CPESs determined from the intensity ratios between ^{1}H NMR peaks at δ 7.8–8.0 (aromatic H's *ortho* to $-SO_2-$) and δ 1.5–1.7 ppm ($-C(CH_3)_2-$) are around 22,000 for both samples.

Miscible blends of HPES (or CPES) and BPADCy were prepared by thoroughly stirring the two components at 130°C under nitrogen atmosphere. The transparent appearance during mixing stage suggests that two components are completely miscible. In case of catalyzed system (CA/NP = 8/100 v/v), the catalyst solution in CH_2Cl_2 was added into the solution of BPADCy and HPES in CH_2Cl_2. The resulting solution was evacuated under reduced pressure and the resulting mixtures were also stirred at 130°C to make miscible blends. Miscible blends thus prepared were further cured at specific temperatures (i.e. 200, 230, or 260°C) for 90 min before post-cure at 280°C for 30 min. During the cure, the originally transparent mixtures became opaque, an indication of gradual phase separation along the progress of cyclotrimerization. Completeness of the curing reaction was confirmed by the disappearance of the infrared absorption peaks at 2200–2300 cm^{-1} ($-C\equiv N$ Stretching). The cured products were then sent for DSC, SEM and TEM investigations.

2.2. Preparations of the miscible blends for optical microscopy

Mixture of HPES/BPADCy was stirred at 130°C and the resulting transparent liquid was withdrawn and placed in between two glass slides for optical microscopy. Generally, one piece of aluminum foil was placed between top and bottom glass slides to control the sample thickness and avoid the shear-induced effect. A Nikon Optiphot-POL

Table 1
Rate expressions for cure of BPADCy and CPESs of different molecular weights

Sample	Rate expression (1/min)[a]
BPADCy	$d\alpha/dt = 1.25\times10^{8}\ (1 + 1.28\alpha)\ \exp(-E_a/RT)$ [b]
CPES-L (910)[c]	$d\alpha/dt = 2.16\times10^{7}\ (1 + 0.19\alpha)\ \exp(-E_a/RT)$ [b]
CPES-M (1550)[c]	$d\alpha/dt = 7.91\times10^{6}\ (1 + 0.012\alpha)\ \exp(-E_a/RT)$ [b]
CPES-H (3240)[c]	$d\alpha/dt = 8.34\times10^{5}\ (1 + 0.008\alpha)\ \exp(-E_a/RT)$ [b]

[a] Rate expression was determined from dynamic DSC analysis.
[b] E_a for BPADCy is 94.8 kJ/mol while for CPESs is 92 kJ/mol.
[c] The number in the bracket refers to the molecular weight determined from ^{1}H NMR.

BPADCy =

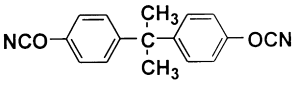

CPES =

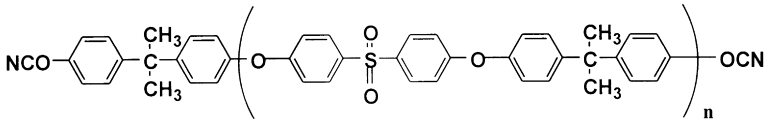

microscope equipped with a THMS 600 hot stage, a Linkam TMS controller, and a Sony video recorder was used to observe the real-time phase separation process. The vision under microscope was sent to a color monitor and the video recorder by a CCD camera. After recording, the videotape was played and the particle sizes in the image can be measured directly on the monitor screen and corrected by a standard scale. A total of 100 particles were counted to obtain the average particle size.

2.3. Instrumentation

A Du-Pont DSC 910 cell connected to a Du-Pont 9900 data station was used. Calibration of the calorimeter was conducted for each heating rate using an indium standard. Miscible blends (~5 mg) prepared according to the above procedures were sealed in the sample pan and heated with a rate of 20°C/min to 200°C for 90 min and 280°C for 30 min. The cured samples thus generated were cooled (cooling rate = 20°C/min) to room temperature before re-scanning to obtain the glass transition temperatures (T_g) values. Again, completeness of curing reaction can be confirmed by the absence of any residual exothermic heat during the second re-san. Proton ^{1}H NMR was studied with a Gemini-200 FT-NMR model. The infrared spectra were obtained from a Digilab FTS-40 FTIR spectrometer. For curing study, sample in a Pyrex holder was sitting in a Pyrex gas cell (diameter = 25 mm, length = 150 mm) connected to thermocouples for temperature control. Fracture surfaces of cured samples were examined using a JEOL JSM-6400 scanning electron microscope at a 20 kV accelerating voltage under secondary electron image mode. Samples were fractured at ambient temperature below T_gs of the corresponding samples. The fracture surfaces were then coated with gold by vapor deposition using a vacuum sputter coater. Based on SEM results, the particle sizes were obtained by taking average values of 100 particles in the fractographs. A JEOL JEM-100S transmission electron microscope was employed to examine the interfaces between the second phase and matrix in the cured CPES/BPADCy. Specimen was embedded in a cured epoxy resin, sectioned to 30–45 nm thick by ultramicrotome of Reichert Ultracut E, and then stained with 1 wt% aqueous solution of ruthenium tetraoxide.

2.4. Sample codes

The starting blends are designated as BH (or C)–*Y* (shown in the first column of Table 1). The first capital B stands for BPADCy, the second H (or C) for HPES

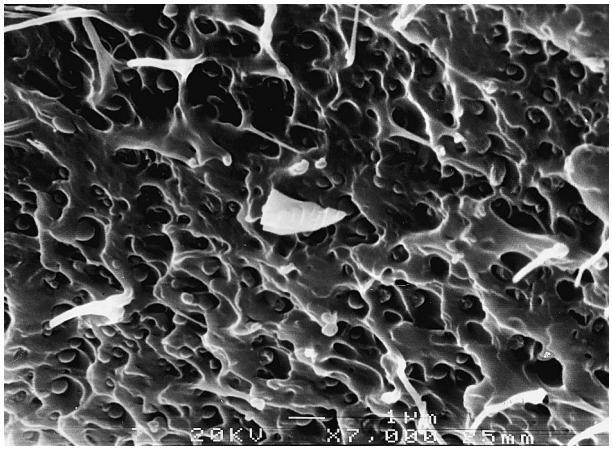

Fig. 2. SEM micrograph of the fracture surface of a cured BH-10. Sample was prepared by curing at 200°C for 90 min and then at 280°C for 30 min.

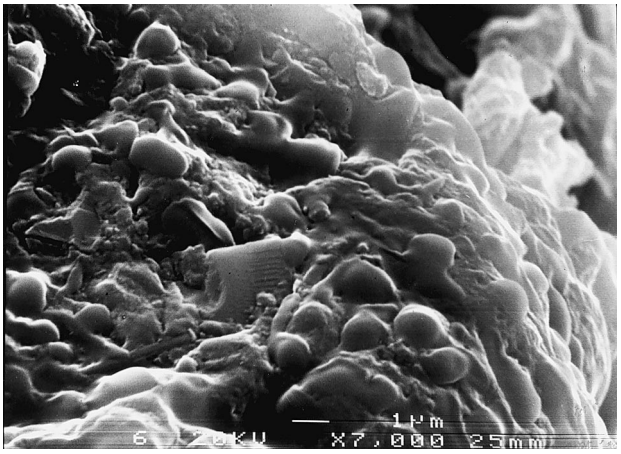

Fig. 3. SEM micrograph of the fracture surface of a cured BC10. Sample was prepared by curing at 200°C for 90 min and then at 280°C for 30 min.

(or CPES), and the number *Y* refers to the weight percentage of the HPES (or CPES) applied in the starting blend. In a catalyzed system, the additional C1 is used to indicate that 1 wt% of the catalyst system was utilized.

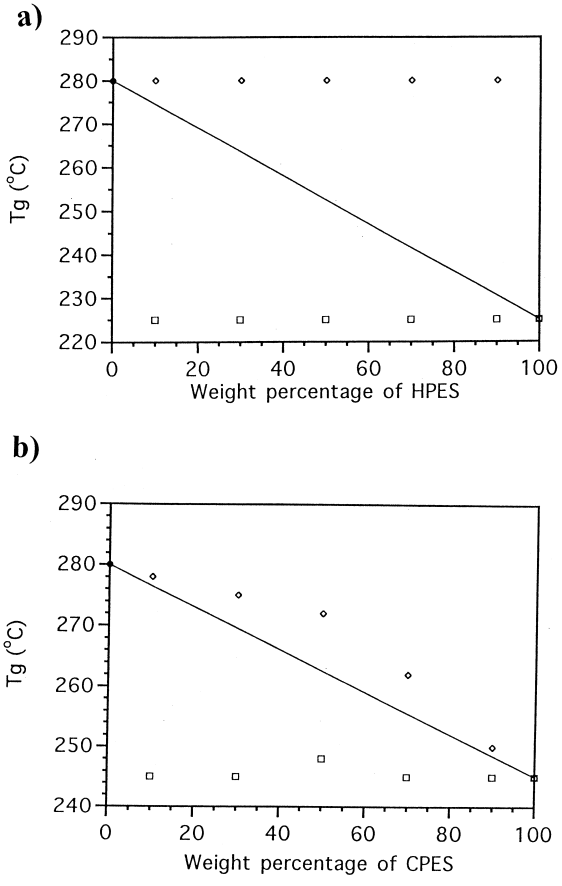

Fig. 4. T_gs versus compositions for: (a) the cured BH-10; and (b) the cured BC-10 systems (the samples were prepared by curing at 200°C for 90 min and 280°C for 30 min).

3. Results and discussion

The fracture surfaces of the cure BH-10 and BC-10 were firstly examined by SEM. The fractograph of the cured BH-10 (Fig. 2) shows the matrix–domain morphology with the matrix phase continuously interconnected and the domain phase present as spherical particles hidden inside the knitted matrix phase. The particle phase can be removed by continuous extraction with methylene chloride, which indicates that this phase is enriched in HPES. The cracks propagated along the particle–matrix boundary, and create obvious cavitation and plastic deformation on the matrix side of the interface. The sharp and clean interface implies that there is no (or weak) interaction between BPADCy and HPES. In contrast to the distinct two-phase morphology in the cured BH-10, morphology of several scattered, globule-like particles coated with blurring interface (Fig. 3) can be observed in the cured BC-10. Existence of interface between particle and matrix will be demonstrated later in this paper by TEM. This blurring interface should result in good adhesion force between the particles and matrix. When fracture occurred at any weak point around the interface, the blurring interface was thus generated.

Glass transition temperatures (T_gs) of the cured BH and BC products also reflected some difference between both systems. T_gs detected by DSC were plotted versus compositions of the cured BH and BC systems in Fig. 4a and b, respectively. The two T_gs observed in Fig. 4a suggests the presence of two phases for all compositions of the cured BH products, a result correlated with the two-phase morphology shown in Fig. 2. Despite the composition difference, all cured BH products exhibited two constant T_gs with their values remained the same with those for the thoroughly cured BPADCy and HPES homopolymer. This result indicates that the extent of phase separation is high for all compositions of the cured BH products.

Results shown in Fig. 4b also suggests the presence of two phases in the cured BC products of all compositions, however, the trend of T_g versus composition is different

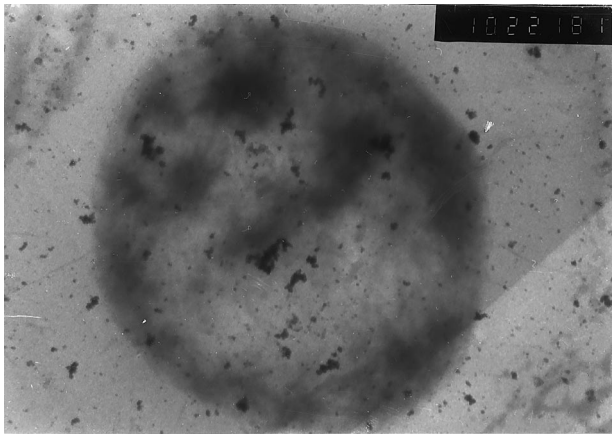

Fig. 5. The particle phase of a cured BC-10 sample from TEM. Sample was prepared by curing at 200°C for 90 min and then at 280°C for 30 min.

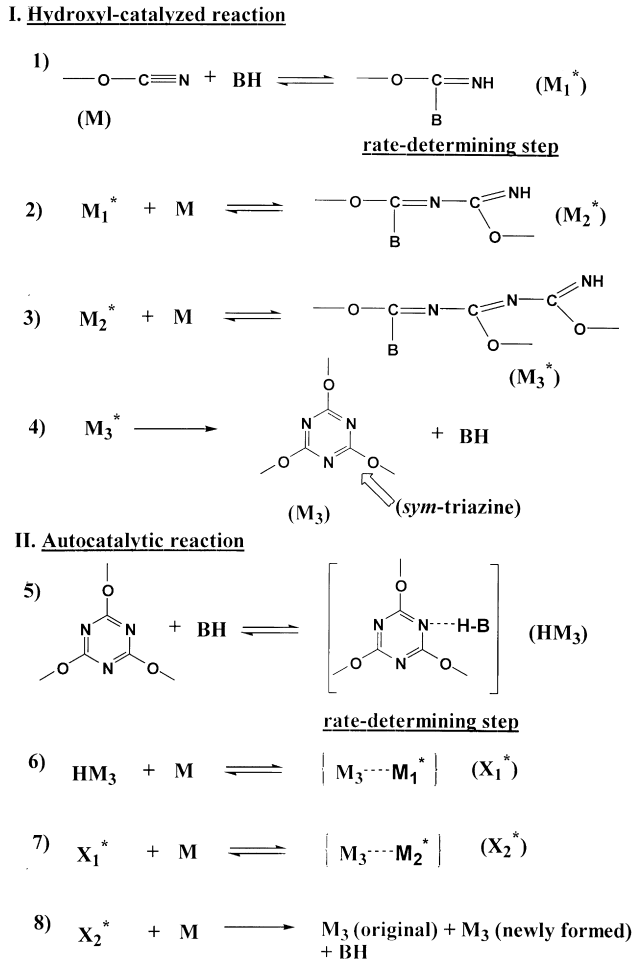

Scheme 1.

from the cured BH system. Here, the T_gs of the BPADCy-rich phases are affected by the co-cured CPES component. As shown in Fig. 4b, the more the CPES amounts applied in the starting blends, the lower the T_gs resulted for the BPADCy-rich phase. On the contrary, the T_gs of the CPES-rich phases are relatively constant despite the variations on the compositions. It seems that certain fractions of CPES components had already incorporated into the network structure of the cured BPADCy and reduced the T_gs of the cured BPADCy-rich phase. On the other hand, the cured BPADCy seems to be difficult to incorporate with the network structure of the cured CPES, which resulted in the constant T_gs of the CPES-rich phase. A plausible explanation will be given later but before that, the blurring interface shown in the cured BC-10 was further examined by TEM.

The TEM micrograph shown in Fig. 5 exhibited two interesting features. Firstly, the globular dark area confirmed that the pieces surrounded by the blurring interface in Fig. 3 are really spherical in shape. Secondly, the surrounding shell is dark. Here, all dark areas in the shell and core regions are enriched in poly(ether sulfone) since the inherent sulfone (–SO_2–) linkage can be selectively attacked by the staining agent, RuO_4. The dark shell confirmed the existence of interface as we observed in the corresponding SEM fractograph in Fig. 3.

The morphological difference between the cured BH and BC systems may be explained in terms of the terminal groups inherent in the HPES and CPES components. Basically, there is no possibility of chemical reaction between HPES and BPADCy during curing; a result correlated with the fact that the hydroxyl terminals in HPES are actually unable to attack the −OC≡N group in BPADCy (this reaction can be made possible with the addition of catalyst system as we will present later). In contrast to the BH system, the inter-reactions between the constituent components in BC blends are highly probable through the polycyclotrimerization of the cyanate groups in the CPES and BPADCy components. The inclusion of poly(ether sulfone) in the BPADCy-rich phase as suggested by the relationship between T_gs and composition can be basically explained by a two distinctive diffusion processes, which are originated from the curing rate difference between CPES and BPADCy as described in the next paragraph.

The original BC blends were transparent in appearance. During curing at ambient temperatures, the partially cured BC systems gradually became opaque, an indication of the progressive phase separation. The phase separation is closely related to the curing rate difference between BPADCy and CPES. Our previous investigation [14] on the curing kinetics and mechanism of BPADCy and CPESs of three molecular weight levels (CPES-L, CPES-M, and CPES-H with M_n of 910, 1550 and 3240, respectively) were summarized in Table 1. Cure of BPADCy and CPES follows the same mechanistic steps of other aromatic dicyanates [15,16], consisting of the hydroxyl-catalyzed and the autocatalyzed paths (Scheme 1) (Mechanistic pathways for polycyclotrimerization of aromatic cyanate group). In the hydroxyl-catalyzed reaction, the aromatic –OCN group was first attacked by the active hydrogen species (BH, most likely the residual phenol group) to generate the M_1^* species (step 1), followed by additions of two –OCN groups (steps 2 and 3) and the final release of BH catalyst to generate the desired *s*-triazine (M_3, step 4) ring. Autocatalytic reaction basically proceeds with the same mechanistic steps as hydroxyl-catalyzed one except in this case, a triazine-bonded BH species (HM_3), instead of pure BH, functions as the nucleophilic species. The alkaline nitrogen atoms in *s*-triazine actually enhance the capability of BH to serve as nucleophile. The first-order autocatalytic rate expression, $d\alpha/dt = Af(\alpha)\,(1 + B\alpha)\exp(-E_a/RT)$, listed in Table 1 was therefore obtained to correlate the mechanism shown in Scheme 1. Here, BPADCy and CPESs possess a similar E_a value (94.8 vs. 92.0 kJ/mol), a result related to the fact that the chemical environments of both cyanate groups in BPADCy and CPES are the same (cyanate groups in BPADCy and CPESs are all connected to the same –Ph–$C(CH_3)$– moieties, cf. the

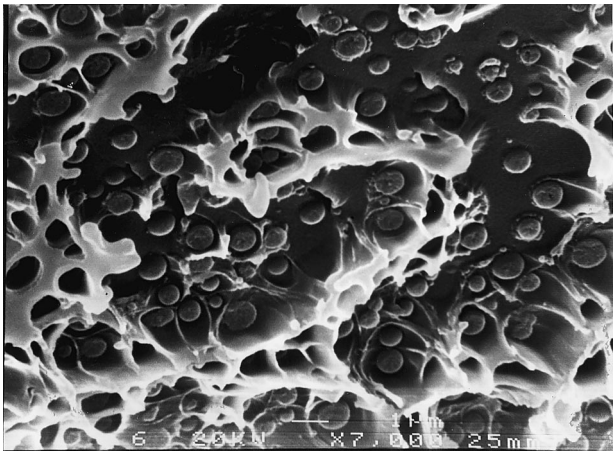

Fig. 6. SEM micrograph of the fracture surface of a cured BH-10. Sample was prepared by curing at 260°C for 90 min and then at 280°C for 30 min.

chemical structures below Table 1). Therefore, the reactivity difference between BPADCy and CPES comes from the distinct concentrations of the active –OCN terminals in BPADCy and CPES. For CPES-L, -M, and -H, the pre-exponential factor, $Af(\alpha)$, and the contribution of the autocatalytic reaction, B, are decreased with increasing molecular weights of CPESs. This can be understood by the decreasing concentration of cyanate terminal with the increasing molecular weight. It is therefore reasonable that BPADCy, with a low-molecular weight (278), would possess a higher curing rate than all other polymers listed Table 1. CPES-H, with the high-molecular weight ($=3240$), has its $Af(\alpha)$ value two orders of magnitude lower than BPADCy. It is conceivable that CPES used in this study, with a higher molecular weight ($M_n = 22,000$) than CPES-H, should have a even lower curing rate than BPADCy. The low curing rate and the low concentration of CPES made the cure of CPES a less potent reaction at the initial curing of BC-10. Therefore, cure of the BPADCy component proceeded preferably at the initial stage and led to formation of the BPADCy-rich domains. Certain portions of unreacted CPES will be ejected from the BPADCy-rich domain due to the concurrent fee energy difference accompanied by the cure process. Visual observation also supported the phase separation process since cure makes the originally transparent BC-10 mixture become opaque gradually. As cure proceeded, certain unreacted CPES were trapped by the network structure in the BPADCy-rich domain. At the later stage, the polycyclotrimerization of CPES became possible since the produced *s*-triazine rings (as the crosslinked points responsible for the autocatalytic reaction [15–17]) would eventually catalyze the less probable reactions of polycyclotrimerizations of CPES and inter-reactions between CPES and BPADCy. These CPES chains entrapped by the network of the BPADCy-rich domain will affect the T_g value of the BPADCy-rich domain. The CPES ejected at the early stage formed the CPES-rich domain, with its boundary shell (as the interface layer shown in Fig. 3) formed, mostly likely, by inter-reaction between CPES and BPADCy.

The effect of curing temperature was evaluated by curing BH-10 at different temperatures (i.e. at 200, 230 or 260°C for 90 min before final cure at 280°C for 30 min). The product cure at 260°C showed a similar matrix–domain

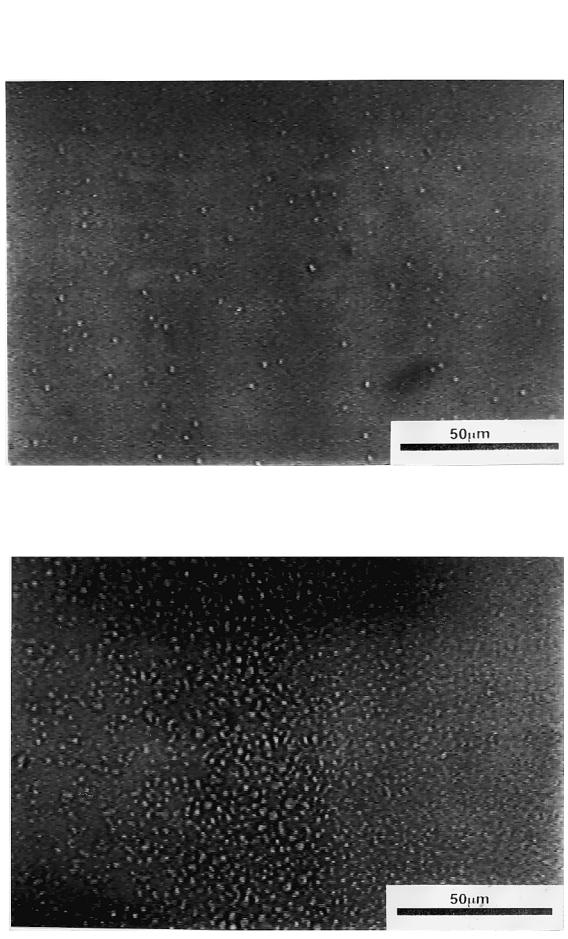

Fig. 7. Transmission light micrographs of BH-10 blend after cure at 200°C for: (a) 16 min 40 s; and (b) 39 min 30 s.

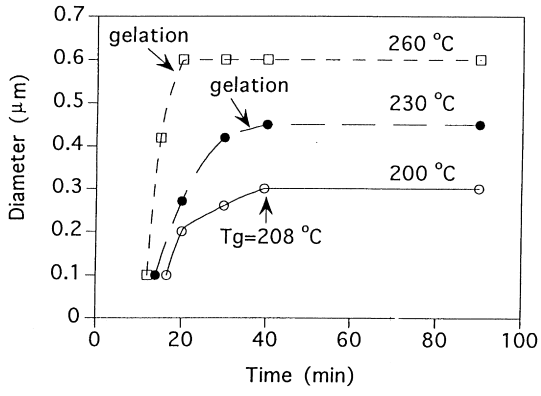

Fig. 8. The average diameter versus isothermal curing time for BH-10 system (the gelation time indicated by the arrows referred to a calculated conversion of 60% for cure of BPADCy).

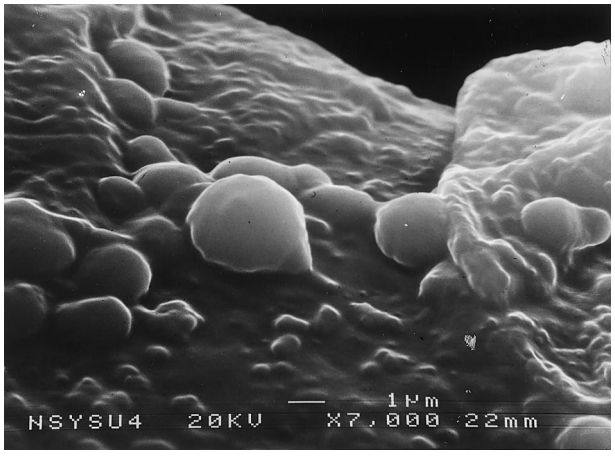

Fig. 9. SEM micrograph of the fracture surface of a cured BH-10C1. Sample was prepared by curing at 200°C for 90 min and then at 280°C for 30 min.

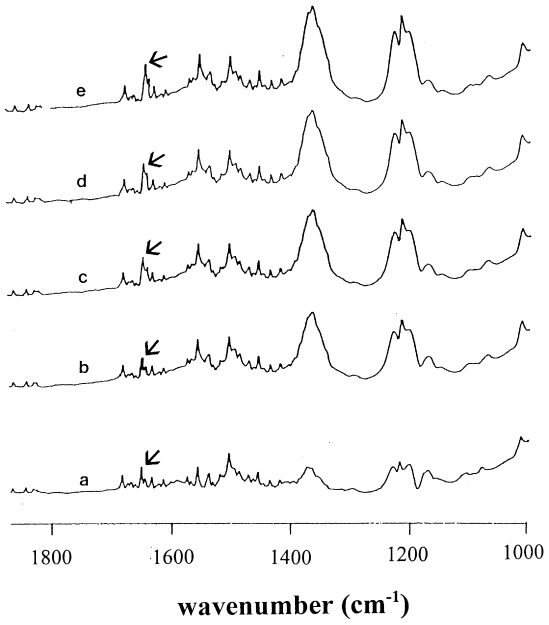

Fig. 10. FTIR spectra of BH-10C1 cured at 200°C for: (a) 0 min; (b) 4 min; (c) 8 min; (d) 16 min; and (e) 32 min.

morphology (Fig. 6) but different particle sizes compared with the sample cured at 200°C. Clearly, a higher curing temperature resulted in a larger particle size (compare Fig. 6 with Fig. 3). Based on SEM results, an average particle size of 0.35 ± 0.03, 0.45 ± 0.05, and 0.65 ± 0.08 μm was resulted from samples pre-cured at 200, 230, and 260°C, respectively. Assuming vitrification is the cause responsible for the structure lock-in, we would expect a smaller particle size for curing at higher temperatures since reaction rate is higher with a higher curing temperature. Therefore, this result is peculiar.

The effect of temperature was further surveyed by a careful real-time optical study, which provides information on the growth and the freezing of the dispersed particles at three temperatures (i.e. 200, 230 and 260°C). Selected optical micrographs in Fig. 7a and b show the real-time phase-separation process during cure of BH-10. The micrograph of BH-10 (Fig. 7a) exhibits the first appearance of spherical droplets after heating at 200°C for 16 min and 40 s. The droplets increased in size initially by growth, later by coalescence (two or more droplets merge into one), and finally became immobilized to result in the final distribution of different particle sizes (Fig. 7b). Average particle diameter can be obtained by averaging the diameters of 100 particles shown in the corresponding micrograph. The results were depicted in Fig. 8, which show the average diameters of the dispersed particles increased initially and then leveled off at a time dependent on the curing temperatures. In cases of 230 and 260°C, the whole specimen became immobilized at a time corresponding to the gel conversion (~60%) reported for most of the aromatic dicyanates [18–21]. This suggests that diffusion of the linear HPES after gel is difficult or impossible to proceed due to the entangled polycyanurate network. In contrast, the freezing of the morphology for the one cured at 200°C occurred at a time (39 min 30 s) well before the gelation. To identify, BH-10 was sealed in a DSC sample pan and heated at 200°C for 39 min 30 s before quenching for the re-scan. This cured sample has a T_g of 208°C (above the curing temperature, 200°C). The result indicates that vitrification instead of gelation plays the crucial role on the morphology developed during cure at 200°C. It is well accepted that the glass transition temperature is an index of chemical reaction during an isothermal cure process of a crosslinkable monomer mixtures, e.g. amine/epoxy system [22]. The glass transition temperature of the uncured reactants is originally low and increases with the chemical conversion during isothermal cure. Isothermal cure of BPADCy at 200°C for 40 min produced pre-gel clusters with their average T_g ($= 208$°C) higher than the curing temperature. Therefore, after curing at 200°C for 40 min, the partially cured BPADCy clusters were situated in the vitrified solid state, in which the corresponding chain mobility was seriously restricted and global translation motion is extremely difficult. It is then suggested that continuous morphological development was arrested because the long HPES chain may be entrapped by the frozen BPADCy-rich matrix at this moment. In summary, the growth of the particle phase before gelation (or vitrification) depends mainly on the diffusion rate of the HPES chains and thermodynamic miscibility. Accordingly, even with less time to develop the HPES-rich phase, cure at 260°C can generate the larger dispersed particles than cure at 230°C (or 200°C) due to the higher diffusion rate of HPES at higher temperature. The ultimate average diameters of the particles obtained from optical microscopy are slightly lower than those obtained from SEM experiments. Samples under SEM inspection were subjected to further post-cure at 280°C for 30 min.

The result indicated further morphological development proceeded during the post-cure stage.

The effect of catalyst was also evaluated. With the addition of 1 wt% CA/NP catalyst, the cured BH-10C1 lost the interconnected structure as the cured BH-10 has. Fig. 9 shows that the cured BH-10C1 possesses a similar picture as the cured BC-10, with scattered particles coated with a layered of blurring interface. The particles sizes, however, seems to be more heterogeneously distributed as compared with the cured BC-10.

As similar to the cured BC-10, formation of interface zone in the cured BH-10C1 may be also attributed to certain kinds of inter-reactions between its constitutive components, HPES and BPADCy. In considering that the only difference between BH-10 and BH-10C1 is the added catalyst, formation of interface in the cured BH-10C1 may be due to the inter-reaction promoted by the added catalyst. The evidence was provided by the corresponding infrared spectra at different temperatures (Fig. 10), which show the presence of absorption at 1650 cm^{-1} (–C=N stretching) in addition to the *s*-triazine absorptions at 1580 and 1370 cm^{-1}. The extra 1650 cm^{-1} band indicated the formation of the iminocarbonate (–O–C(=NH)–O–) [23,24] bond through the reaction of hydroxyl termini in HPES and the cyanate groups in BPADCy. The reaction had been reported to be catalyzed by the alkaline potassium *t*-butoxide [23]. With organometallic catalysts as in our case, formation of iminocarbonate bonds through inter-reaction between HPES and BPADCy seems to be greatly promoted in comparison to the non-catalyzed BH-10 system, in which the absence of inter-reaction resulted in the failure of formation of an interfacial zone. Heterogeneity on the final particle sizes may be connected to the distribution of the catalyst applied in the starting BH-10C1 blend.

4. Conclusion

Based on the experimental results in this study, three statements can be addressed here.

(1) Fractographs of the cured BH-10 and BC-10 showed major difference in the domain–matrix interfaces. Use of CPES resulted in a material with an extra interface between the particles and matrix phases.

(2) The resulting particle sizes in the cured BH-10 strongly depend on the curing temperature. The higher the curing temperatures, the larger the resulting particles.

(3) Addition of catalyst system created interfacial zones between particles and matrix phases because of the generation of iminocarbonate bonds through the promoted inter-reactions between the constituent components, HPES and BPADCy.

Acknowledgements

We appreciate the financial support of National Science Council, ROC, under contract no. NSC 86-2216-E-110-004.

References

[1] Grigat E, Putter R. Angew Chem Int Ed 1967;6:206.
[2] Grigat E, Putter R. Chem Ber 1964;97:3012.
[3] Ayano S. Chem Econ Engng Rev 1978;10:25.
[4] Cozzens RF, Walter P. J Appl Polym Sci 1987;34:601.
[5] Osei-Owusu A, Martin GC. Polym Mat Sci Engng 1991;35:304.
[6] Gotro JT, Appelt BK, Papathomas KI. Polym Compos 1987;8:39.
[7] Mark HF, Kroschwitz JI. Encyclopedia of polymer science and engineering, vol. 8. New York: Wiley, 1988.
[8] Wertz DH, Prevorsek DC. Polym Engng Sci 1985;25:804.
[9] Wertz DH, Prevorsek DC. ANTEK 84, Proceedings of the 42nd Technical Conference and Exhibition, 1884, p. 804.
[10] Feldman JA, Huang S. Crosslinked Polymer, ACS Symposium Series 367. Washington DC: American Chemical Society, 1988.
[11] Cao ZO, Mechin F, Pascault JP. Polym Int 1994;34:41.
[12] Woo EM, Shimp DA, Seferis JC. Polymer 1994;35:1658.
[13] Woo EM, Su CC, Kuo JF, Seferis JC. Macromolecules 1994;27:5291.
[14] Chang JY, Hong JL. Macomol Chem Phys 1995;196:3753.
[15] Wang YH, Hong YL, Hong JL. J Appl Polym Sci 1995;58:1585.
[16] Lin RH, Hong JL, Su AC. Polymer 1995;36:3349.
[17] Lin RH, Su AC, Hong JL. J Polym Res 1997;4:191.
[18] Simon SL, Giham JK, Shimp DA. Polym Mater Sci Engng 1990;62:96.
[19] Bauer M, Bauer J, Kuhn G. Acta Polym 1986;37:715.
[20] Bauer J, Lang P, Burchard W, Bauer M. Macromolecules 1991;24:2634.
[21] Gupta AM, Macosko CW. Macromolecules 1993;26:2455.
[22] Wisanrakkit G, Gillham JK. J Coatings Tech 1990;62:35.
[23] Kohn AM, Langer R. Biomaterials 1986;7:176.
[24] Grigat E, Putter R. Chem Ber 1964;197:3022.